Targeting the Force-Displacement Response of Thin-walled Structures Subjected to Crushing Load using Curve Decomposition and Topometry Optimization

Xu Han[a], Weigang An[a,*], Andres Tovar[b]

[a] *College of Aeronautics, Northwestern Polytechnical University, Xi'an 710072, China*
[b] *Department of Mechanical and Energy Engineering Indiana University-Purdue University, Indianapolis 723 W Michigan St, SL 260N, Indianapolis, IN 46202-5132, USA*
[*] *Corresponding Author. Tel: 13572995257. E-mail: anweigang@nwpu.edu.cn*

Abstract

This work introduces a new approach to targeting the dynamic response of thin-walled energy absorbing structures through the decomposition of the force-displacement (FD) response and the use of topometry (thickness) optimization. The proposed method divides the non-linear optimization problem into a series of analytical subproblems. In each iteration, an explicit dynamic analysis is carried out and the dynamic response of the structure is then used to define the subproblem. Numerical examples show that the algorithm can tailor the FD response of the structure to a target FD curve. Progressive collapse, which is a high-energy collapse mode and desired in design for crashworthy, is observed in the optimized thin-walled structures. The proposed algorithm is computationally efficient as uses a fewer explicit simulations to reach the target response.

Keywords: Topometry Optimization; Force-Displacement Response; Crashworthiness Optimization; Design for Crashworthiness

1. Introduction

Thin-walled structures are widely used in the automobile and aviation industries due to their lightweight, manufacturability, and impact energy absorbing capabilities (Baroutaji et al. 2017). When a car or a plane crashes, thin-walled structures can provide occupant safety by dissipating energy through their progressive collapse as observed in axially impacted tubes (rails and crashboxes) (Zeng and Duddeck 2017, Guler et al. 2010). A low-energy collapse mode is global bending, which must be avoided (Jones 1997). Therefore, understanding this collapse mode also requires attention in design of thin-walled structures. Currently, finite element based-optimization methods, particularly topometry (thickness) optimization methods, are being developed to tailor the dynamic structure response under dynamic crushing loads.

The concept of topometry optimization, coined by Leiva (2004), is a generalized sizing optimization approach in which the finite element model of the thin-walled structure

is used in conjunction with specialized optimization algorithms in order to find the optimal thickness of each finite element in the model. As noted by Duddeck et al. (2016), the majority of the topometry optimization algorithms can only handle linear or mildly-nonlinear models under static loading conditions; only a handful of algorithms can handle fully nonlinear models under dynamic load. Two algorithms for nonlinear structures that are usually compared are the Equivalent Static Load (ESL) method (Kim and Park 2010, Park 2011, Park and Kang 2003, Shin et al. 2007) available in the commercial code GENESIS (VR&D, Colorado, USA) and the Hybrid Cellular Automaton (HCA) method (Patel 2007, Patel et al. 2009, Penninger et al. 2010, Penninger et al. 2013, Tovar et al. 2006) available in the commercial code LS-TaSC (LSTC, California, USA).

In the ESL method, equivalent static loads are defined in a linear model that generate the same response than the dynamic loads on nonlinear model. The optimization of the nonlinear, dynamic model is conducted by the recurrent optimization of equivalent linear static models. This approach has been used, for example, by Witowski et al. (2014) in the design of the inner hood panel of the car.

The HCA method, introduced by Tovar (2004), is inspired by the biological process of bone remodeling. This algorithm utilizes a distributed control algorithm to uniformly distribute a field variable such as internal energy density across the structure. The HCA method has been used to improve crashworthiness indicators in thin-walled vehicle components. For example, Mozumder et al. (2012) developed the HCA method for the topometry optimization of sheet metal structures for impact energy dissipation. Bandi et al. (2015) made use of the HCA method for the topometry optimization of compliant thin-walled tubular structures that progressively collapse under axial load.

The methods such as ESL and HCA are relevant in the design of thin-walled structures for crashworthiness, particularly to increase impact energy absorption, however the other primary crashworthiness indicators such as peak crushing force, maximum deceleration, dynamic penetration, and crash load efficiency have not been considered and need to be addressed. Pedersen (2003) proposed a methodology for designing two-dimensional frames for a desired energy absorption history based on the ground structure method. The ground structure consists of rectangular 2D-beam elements with plastic hinges. A quasi-static nonlinear finite element solution is obtained with an implicit backward Euler algorithm, and the analytical sensitivities are computed by the direct differentiation method. Unfortunately, ground structures are unable to capture the complexity of a continuous 3D shell. Mozumder at. el. (2010) proposed an HCA-based method for topometry optimization using a target force-displacement (FD) response as the design objective. In their research, the FD curve is discretized into several design points and the structure is divided into same number of sub-domains. The sub-domains deform and crush according to the requirements of the FD curve. This is done by adjusting the setpoint so that the error between the actual and target FD response is minimized. The method is likely effective, but the definition of

the sub-domains is rather heuristic and hence it cannot be systematically applied to an arbitrary design problem. This leads to develop topometry optimization methods for continuum structures and their corresponding dynamic responses.

This paper introduces a sequential optimization method that takes elements of both ESL and HCA in order to tailor the FD response of a thin-walled structure subjected to an arbitrary crushing load. The proposed method divides the original optimization problem into a series of subproblems. In each iteration, an explicit dynamic analysis is first carried out and then the dynamic response of the structure is used to define the subproblem. During the iterative process, the thickness of all the elements in the model is updated through the solution of the subproblems. The optimal thickness distribution of the structure is obtained at convergence. An advantage with respect to the preliminary work presented by Mozumder at el. (2010) is that the proposed method does not require the heuristic definition of subdomains within the structure. The effectiveness of the proposed method is demonstrated with the design of squared thin-walled tubular structure subjected to different load case and different target FD responses. The examples show the effectiveness of the algorithm finding the element thickness distribution to make the structure's FD curve gradually approach the target FD curve. The results show how the error between the real and target FD curves is minimized. In this way, by setting a proper target FD curve, the proposed method can improve several crashworthiness indicators including specific energy absorption, peak crushing force, maximum deceleration, dynamic penetration, and crash load efficiency.

The paper is organized as follows: Sec. 2 states the design optimization problem; Sec. 3 presents the proposed optimization method; Sec. 4 shows numerical examples; and Sec. 5 summarizes the work and contributions, and discusses future developments.

2. Optimization Problem Statement

The optimization problem involves two force-displacement (FD) responses of the structure: the target response $F^*(d)$ and the actual response $F(d)$ (Figure 1). The error between the two FD responses corresponds to the objective function to be minimized. This is,

$$\min \quad C = \frac{\int_{d_s}^{d_e} [F(d) - F^*(d)]^2 \, \mathrm{d}d}{d_e - d_s} \tag{1}$$

where d_s and d_e represent the initial and final displacements considered in the simulation, respectively.
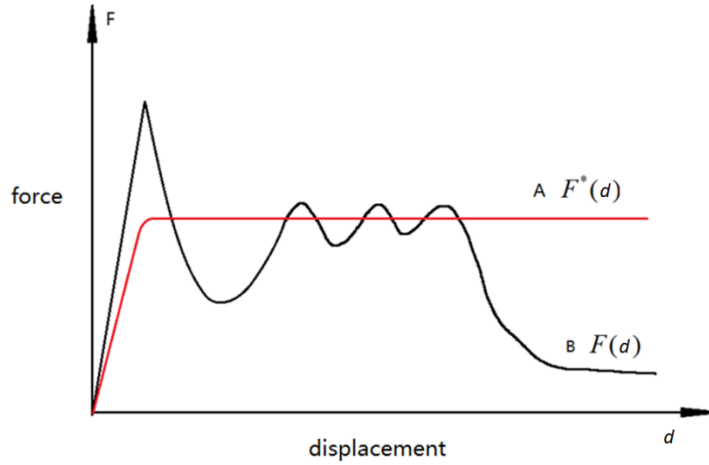
Figure 1: Force-displacement responses of a thin-walled structure subjected to crushing load:
(A) target FD response, (B) actual FD response.

Due to the discrete nature of the numerical analysis, the objective function (1) is transformed from a continuous integral form to a discrete summation form. To this end, a series of discrete (equidistant) displacement points $d_1, d_2 ..., d_m$ are defined on the interval $[d_s, d_e]$ to discretize the FD curve into m design points (Figure 2). Thus, the objective function (1) can be restated as

$$\min \quad C(\mathbf{d}) = \frac{1}{m} \sum_{j=1}^{m} [F(d_j) - F^*(d_j)]^2 \tag{2}$$

where $\mathbf{d}$ is the vector of displacement points $\mathbf{d} = [d_1, d_2 ..., d_m]$.
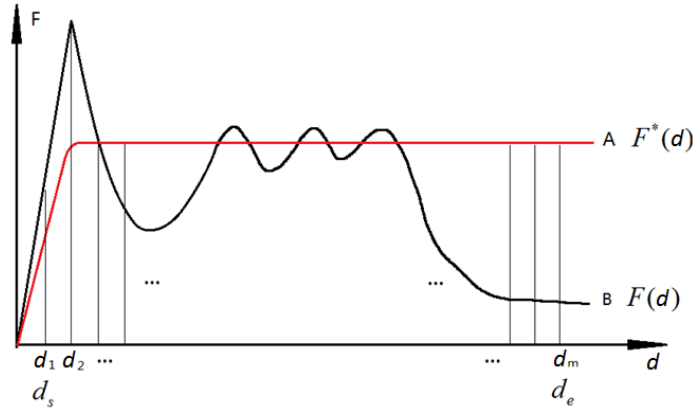

Figure 2: Displacement points discretizing the FD target and actual curves.

The thickness of each finite element is taken as the design variable $t^{(e)}$. The mathematical statement of the optimization problem is as follows:

4

$$\text{find} \quad \mathbf{t} \in \mathbb{R}^N$$

$$\min \quad C(\mathbf{d}, \mathbf{t}) = \frac{1}{m} \sum_{j=1}^{m} \left[F(d_j, \mathbf{t}) - F^*(d_j) \right]^2 \tag{3}$$

$$\text{s.t.} \quad t_{min} \leq t^{(e)} \leq t_{max}, \quad e = 1, \dots, N$$

where $\mathbf{t}$ is the vector of element thickness values, $\mathbf{t} = [t^{(1)}, \dots, t^{(N)}]$, e is element number, N is total number of elements, m is the number of the displacement points, and t_{min} and t_{max} are lower and upper bounds, respectively.

3. Optimization Procedure

3.1 Framework of the algorithm

In order to solve the problem defined in (3) using a traditional gradient-based optimization algorithm, the sensitivity of $C(\mathbf{d}, \mathbf{t})$ with respect to the thickness of each element $t^{(e)}$ should be approximated. Unfortunately, there is no closed-form, analytical expression that considers all the nonlinearities of the finite element model, i.e., large displacement, inelasticity, and contact. Furthermore, a numerical approximation through finite differences methods is impractical due to the computational cost of the simulation and the large number of design variables. Therefore, the use of a gradient-based optimization algorithm is impractical and an alternate method is required.

In this paper, a heuristic method is introduced. In this method, each iteration consists of one explicit dynamic analysis and the solution of a subproblem. The explicit dynamic analysis provides parameters to define the subproblem—i.e., nodal displacement and the element (internal and kinetic) energy rates as a function of time. In the subproblem, an approximation method is used to establish an analytical relationship between the objective function and the thickness of each shell element. Thus, the original optimization problem is transformed into a series of simpler subproblems (Sec. 3.4). The steps involved in this algorithm are the following:

Step 1: Prepare the initial finite element model. Define target force-displacement curve $F^*(d)$ and partition into discrete displacements d_j, $j = 1, \dots, m$. Define the thin-walled structure initial (uniform) thickness distribution $\mathbf{t}_{(k)} \in \mathbb{R}^N$ for $k = 0$.

Step 2: Perform explicit dynamics analysis and obtain the actual force-displacement curve $F(d_j, \mathbf{t}_{(k)})$. Evaluate the objective function $C(\mathbf{d}, \mathbf{t}_{(k)}) = 1/m \sum_{j=1}^{m} \left[F(d_j, \mathbf{t}_{(k)}) - F^*(d_j) \right]^2$. Obtain the element derivatives of the kinetic energy and internal energy $R_{EK}^{(e)}(d_j, \mathbf{t}_{(k)})$ and $R_{EI}^{(e)}(d_j, \mathbf{t}_{(k)})$ (Sec. 3.3).

Step 3: Update iteration $k \leftarrow k + 1$. Solve the optimization subproblem (14) (Sec. 3.4). Update the element thickness values (design variables) $\mathbf{t}_{(k)} = \mathbf{t}^*_{(k)}$.

Step 4: If the convergence condition (15) is satisfied (Sec. 3.5) then terminate; otherwise, go to Step 2.

3.2 Derivation of the subproblem objective

In order to derive the objective function of the subproblem, let us analyze the relation between the objective function in (3) and the kinetic and internal energy expressions in each element. When the displacement of the impactor increases from d to $d + \Delta d$, the corresponding increment of the work of the external force is given by

$$\Delta W = \int_{d}^{d+\Delta d} F(d)\mathrm{d}d \tag{4}$$

This work increment is converted to the increment of structural total energy (kinetic energy and internal energy),

$$\Delta W = \Delta E_K + \Delta E_I \tag{5}$$

When $\Delta d \to 0$, then $\Delta W \approx F(d)\Delta d$, which yields

$$F(d) = \lim_{\Delta d \to 0} \left(\frac{\Delta E_K}{\Delta d} + \frac{\Delta E_I}{\Delta d}\right) = R_{EK}(d) + R_{EI}(d) \tag{6}$$

where R_{EK} and R_{EI} are the derivatives of the kinetic energy and internal energy with respect to the displacement d. Therefore, the external force $F(d)$ can be expressed by the sum of the element derivatives of the kinetic and internal energies as

$$F(d) = \sum_{e=1}^{N}\left[R_{EK}^{(e)}(d) + R_{EI}^{(e)}(d)\right] \tag{7}$$

Therefore, the objective function of the subproblem can be expressed as:

$$\min \ C_{(k)}(\mathbf{d}, \mathbf{t}) = \frac{1}{m}\sum_{j=1}^{m}\left\{\sum_{e=1}^{N}\left[R_{EK}^{(e)}(d_j, \mathbf{t}) + R_{EI}^{(e)}(d_j, \mathbf{t})\right] - F^*(d_j)\right\}^2 \tag{8}$$

Analytical forms of $R_{EK}^{(e)}$ and $R_{EI}^{(e)}$ as a function of the element thickness $t_{(k)}^{(e)}$ can be derived in order to minimize (8). This procedure is discussed in the next section.

3.3 Analytical forms of energy derivatives

The derivative of the element kinetic energy is proportional to the change in the element thickness. Then, the following analytical form can be proposed:

$$R_{EK}^{(e)}\left(d_j, t_{(k)}^{(e)}\right) \approx R_{EK(k-1)}^{(e)}\left(\frac{t_{(k)}^{(e)}}{t_{(k-1)}^{(e)}}\right) \tag{9}$$

6

where $R^{(e)}_{EK(k-1)} = R^{(e)}_{EK}(d_j, \mathbf{t}_{(k-1)})$, which remains constant in iteration k, and $\mathbf{t}_{(k-1)} = [t^{(1)}_{(k-1)}, \ldots, t^{(N)}_{(k-1)}]$ is the optimal thickness obtained by the subproblem of iteration $k-1$, which also remains constant in iteration k. The relation between the element's internal energy and its thickness is somewhat more involved. When the structure is subjected to a crushing load, it undergoes large plastic deformation. In that case, the plastic strain is much larger than the elastic strain, so the latter can be neglected (Lu and Yu 2003). Effectively, the material Young's modulus can be taken as infinite, so that the structure exhibits rigid behavior before yielding. In this work, a rigid, perfectly plastic material model is used.

In thin-walled structures, the rigid, perfectly plastic material model results in their plastic deformation being concentrated at discrete, plastic hinge-lines (Figure 3). Along the plastic hinge-lines, the magnitude of the bending moment per unit length must be equal to the fully plastic bending moment per unit length defined as $M_o = \sigma_s t^2/4$, where σ_s is the stress along the plastic hinge-line and t is the thickness.
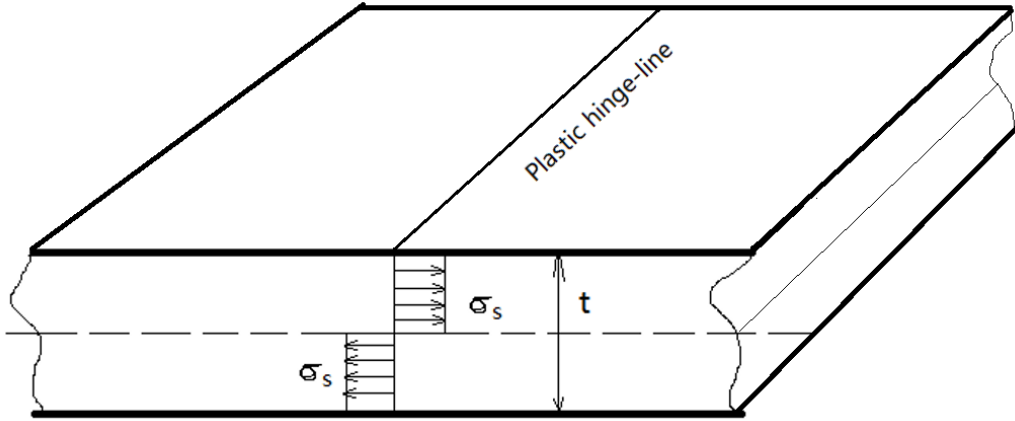

Figure 3: Stress profile across the plastic hinge-line using the rigid, perfectly plastic material model.

For a given relative rotation θ along plastic hinge-line of length L, the total energy dissipation can be calculated by

$$E_I = M_o \theta L = \frac{\sigma_s \theta L}{4} t^2 \tag{10}$$

Then, one can observe that the derivative of the element internal energy is approximately a quadratic function with respect to its thickness. This is,

$$R^{(e)}_{EI}\left(d_j, t^{(e)}_{(k)}\right) = a \left(t^{(e)}_{(k)}\right)^2 \tag{11}$$

where the coefficient a can be obtained from the relation

$$R_{EI(k-1)}^{(e)} = a \left(t_{(k-1)}^{(e)} \right)^2 \tag{12}$$

where $R_{EI(k-1)}^{(e)} = R_{EI}^{(e)}(d_j, \mathbf{t}_{(k-1)})$, which remains constant in iteration k. Finally, one can state that

$$R_{EI}^{(e)} \left(d_j, t_{(k)}^{(e)} \right) \approx R_{EI(k-1)}^{(e)} \left(\frac{t_{(k)}^{(e)}}{t_{(k-1)}^{(e)}} \right)^2 \tag{13}$$

3.4 Subproblem statement

The subproblem can be defined from the analytical relationship between the optimization objective and the energy of elements (Sec. 3.2) and the analytical relationship between design variables and the energy of elements (Sec. 3.3). From equations (8), (9), and (13), the subproblem can be derived and stated as:

find $\quad \mathbf{t}_{(k)} \in \mathbb{R}^N$

$$\min \quad C_{(k)}\left(\mathbf{d}, \mathbf{t}_{(k)}\right) = \frac{1}{m} \sum_{j=1}^{m} \left\{ \sum_{e=1}^{N} \left[R_{EK(k-1)}^{(e)} \left(\frac{t_{(k)}^{(e)}}{t_{(k-1)}^{(e)}} \right) + R_{EI(k-1)}^{(e)} \left(\frac{t_{(k)}^{(e)}}{t_{(k-1)}^{(e)}} \right)^2 \right] - F^*(d_j) \right\}^2$$

$$\text{s.t.} \quad \left| t_{(k)}^{(e)} - t_{(k-1)}^{(e)} \right| \leq \varepsilon, \quad e = 1, \dots, N$$

$$\tag{14}$$

where the parameter ε is the move limit. The solution of subproblem (14) allows to update of the thickness $\mathbf{t}_{(k)}^*$. The iterative process continues until a convergence criterion is satisfied (Sec. 3.5). In some cases, it is advantageous to use a symmetry condition to obtain symmetric structures. When such a condition is used, symmetric elements are grouped and assigned their average thickness value.

3.5 Convergence criterion

The convergence condition is satisfied when

$$\min\{C_{k-N_c+1}, C_{k-N_c+2}, \dots, C_k\} > C_{k-N_c} \tag{15}$$

where N_c is an integer called convergence number, and $k > N_c$ is the iteration number. This means that if the objective function does not decrease in more than N_c iterations, the optimization process is terminated. Due to the numerical noise in explicit dynamic analysis, a typical value of the convergence number is around $N_c = 10$.

3.6 Flowchart of the proposed algorithm

The proposed algorithm is summarized in the flowchart below (Figure 4). Several numerical examples show the effectiveness of this algorithm to match a target FD curve.
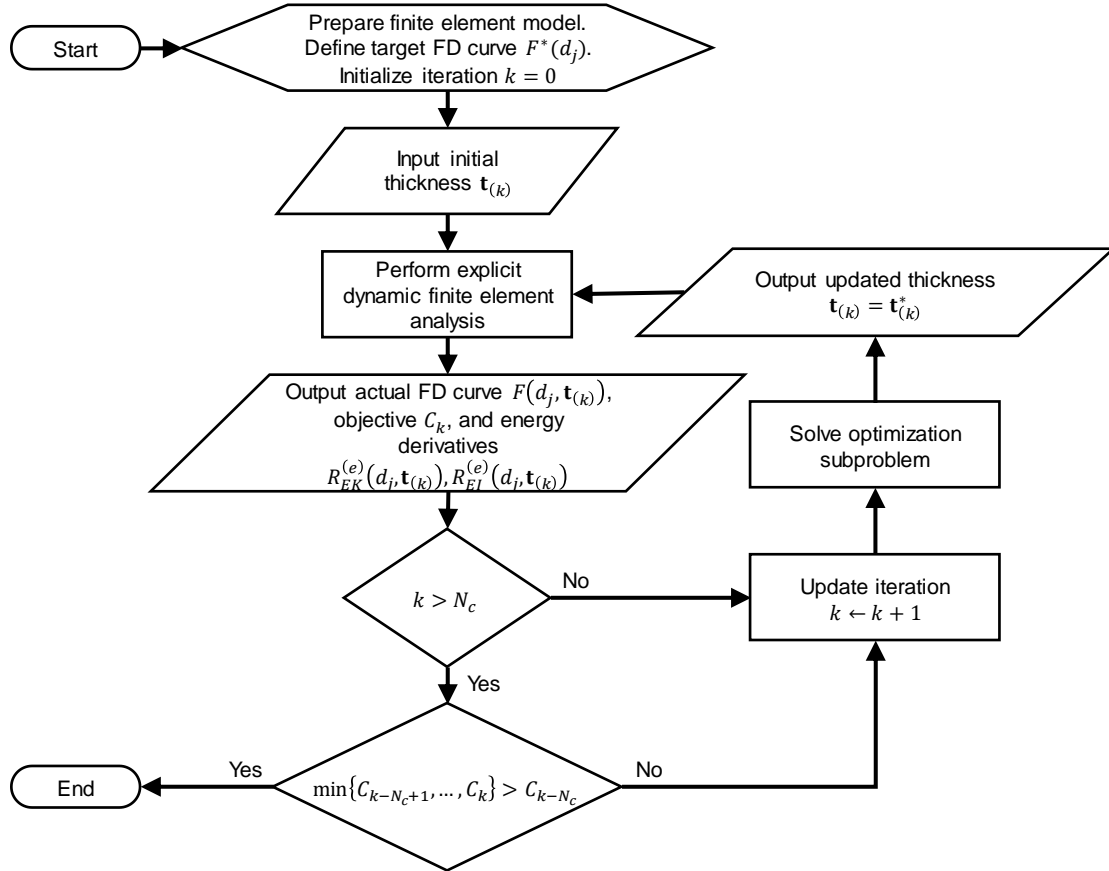

Figure 4: Flowchart of the proposed algorithm.

4. Numerical Examples

In the following examples, thin-walled tubes with different load conditions and target FD curves are optimized. The explicit nonlinear finite element code LS-DYNA is used to perform explicit dynamic analysis (Hallquist 2006). The FE model of the tubes is comprised of fully integrated shell elements (ELFORM=16) with four in-plane integration points, which makes them free of hourglass deformation (Hallquist 2006). Five integration points are used throughout the thickness in order to capture the local element bending accurately. A linear elastic, piecewise linear plastic material (MAT24) is utilized. The material properties correspond to the ones of steel (Table 1). Fracture is not considered.

Table 1: Material properties of the thin-walled tubular structure.

Property	Value
Density	1800 kg/m^3
Young's modulus	207 GPa
Poisson's ratio	0.29
Yield strength	253 MPa
Effective plastic strain	Effective stress (MPa)
0.000	253
0.048	367
0.108	420
0.148	442
0.208	468
0.407	524
0.607	561
0.987	608

Three target FD curves have been used in the examples, namely, straight line, straight line with slope, and power line (Figure 5). The straight line target is defined as

$$F^*(d) = f \tag{16a}$$

where f is the constant force. The straight line target with slope is defined as

$$F^*(d) = \max\left\{\frac{f}{d_t}d, f\right\} \tag{16b}$$

where d_t is the displacement before the force plateau. Finally, the power line target is

$$F^*(d) = \frac{f}{d_t^p}d^p \tag{16c}$$

where d_e is the final displacement and p is the power.

(a) straight line   (b) straight line with slope   (c) power line
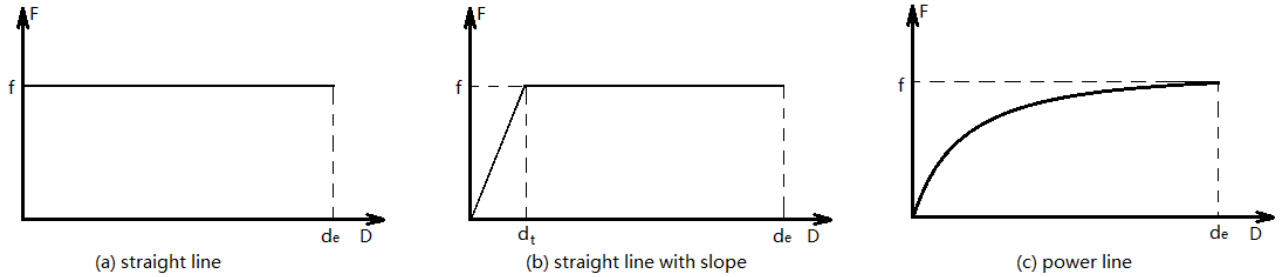
Figure 5: Target FD curves considered in the numerical examples.

The following sections show the results of the application of the proposed algorithm

in the design of a thin-walled square under axial and oblique impact. Similar applications can be observed in the design of vehicle rails and crashboxes. In these examples, the three types of target FD curves are considered: a straight line (axial impact), straight line with a slope (oblique impact), and power line (oblique impact).

4.1 Straight-line FD target under axial impact

Let us consider a thin-walled square tube of length 1.0 m and the side 0.1 m that is fully constrained at the back-end and subjected to an axial impact on the front-end (Figure 6). The impacting rigid plate moves at a constant speed of 5 m/s along the longitudinal axis (y-axis) of the tube, compressing the tube a distance of 0.7 m.
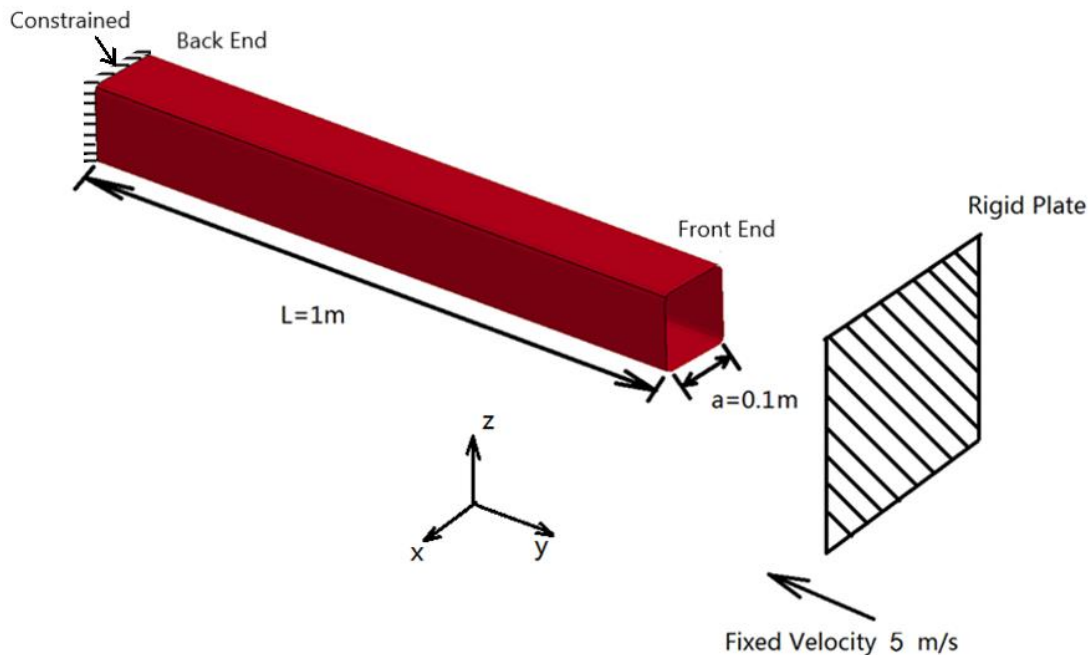
Figure 6: Model setup of the thin-walled square tube under axial impact.

The target FD curve is set as a straight-line type with $f = 200$ kN (Figure 5a). The number of the discrete equidistant displacement points is $m = 700$. Symmetry conditions in directions x and z are added. All elements in the model are square shells with side 10 mm. The thickness of shell elements is chosen as design variables, therefore, there are 4000 thickness variables. The upper and lower bounds of the thickness variables is 6.0 mm and 0.6 mm, respectively. The initial value of thickness variables is 3.3 mm; thus, the initial design is a tube with uniform thickness of 3.3 mm. The limit of the change of thickness in subproblem is $\varepsilon = 0.1$ mm and the convergence number is $N_c = 10$.

The iterative progress of the objective function is shown in Figure 7. The best design

11

is found at iteration 25. The optimization is terminated after 35 iterations. The minimum and maximum values of thickness variables with no. of iterations is shown in Figure 8.
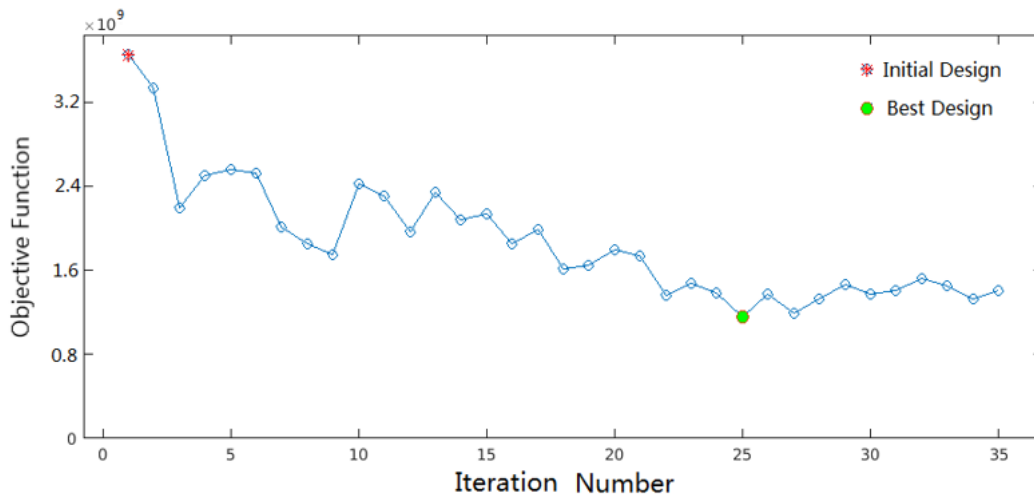

Figure 7: Objective function vs. number of iterations for the straight-line FD target under axial impact.
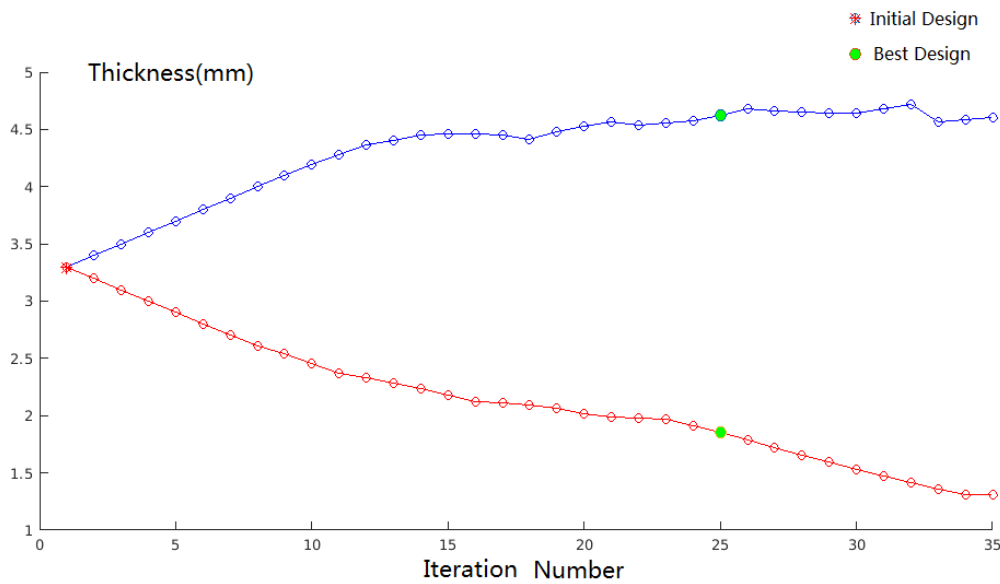

Figure 8: Maximum and minimum thickness values vs. number of iterations for the straight-line FD target under axial impact. At convergence, the minimum and maximum thickness values are 1.85 mm and 4.63 mm, respectively.

The thickness variables of the best design are used to build the design tube, and the designed tube's thickness distribution is shown in Figure 9. The designed tube has a trigger-like, crush initiator mechanism corresponding to two thinner zones in the front end. This feature induces a local buckling at the front end of the tube and the buckling load is

relatively small. The deformation history of uniform thickness tube and designed tube are shown in Figure 10. During pure axial crushing of a thin-walled square tube, the progressive collapse is manifested with the sequential formation of folds from the front-end to back-end of the tube. Comparing the overall deformation of tubes before and after optimization, one finds that a uniformity in the shape and size of each fold of the designed tube.
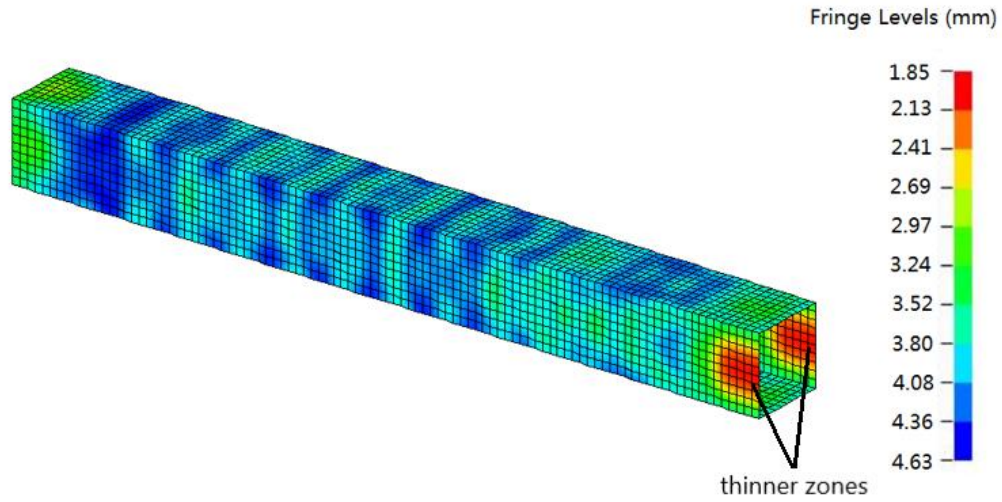

Figure 9: Thickness distribution of the final designed tube for the straight-line FD target under axial impact.
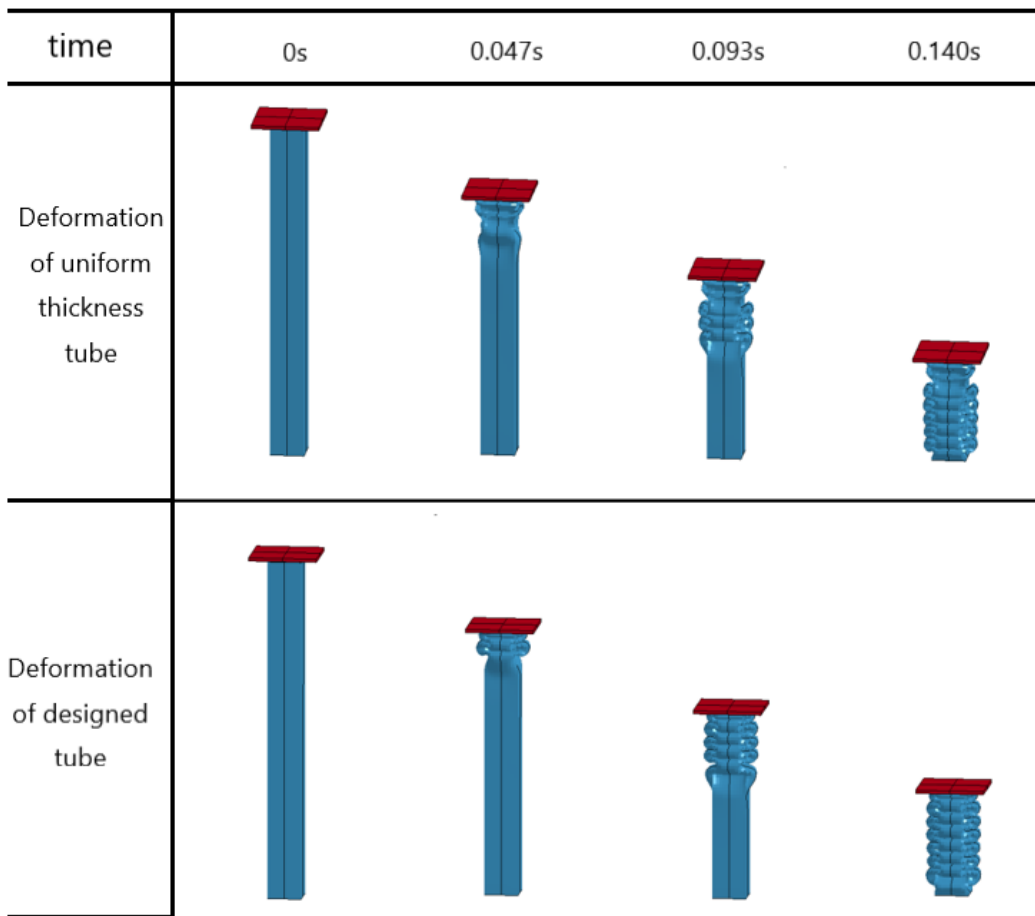
Figure 10: Deformation of the initial uniform-thickness tube vs. the final designed tube for the straight-line FD target under axial impact.

The FD curve of uniform thickness tube and designed tube are shown in Figure 11. The initial peak crushing force of designed tube is lower than the one of the initial design. The FD curve of designed tube more stable and hovers near the target FD curve; therefore, the mean force and other crashworthiness parameters increase. The peak crushing force (PCF), mean force, crash load efficiency (CLE), and specific energy absorption (SEA) of the uniform thickness tube and designed tube are listed in Table 2.
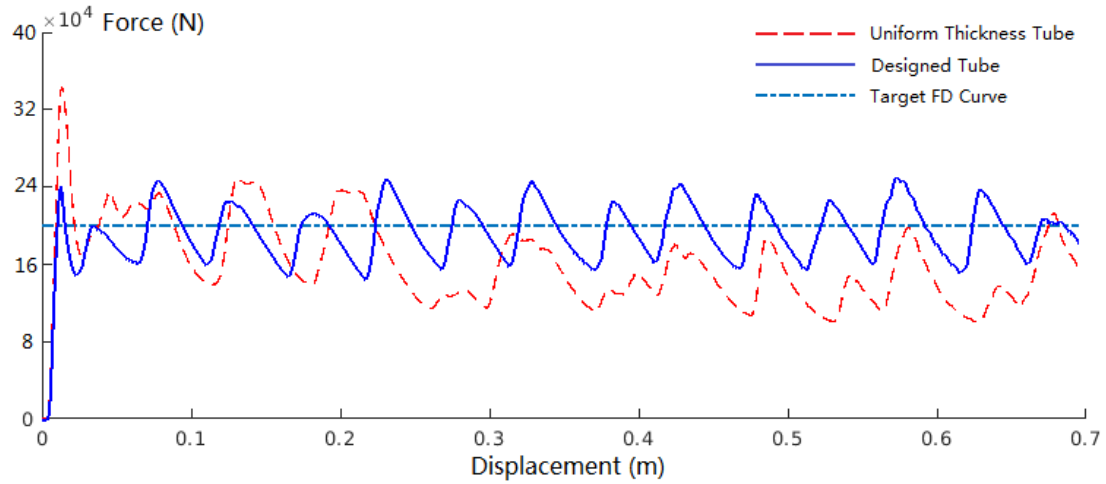
Figure 11: Comparison of the FD responses of the initial and final designs for a straight-line FD target under axial impact.

Table 2: Performance of the initial uniform-thickness tube and the final designed tube for a straight-line FD target under axial impact.

	PCF (kN)	Mean Force (kN)	CLE	SEA (kJ/kg)
Initial uniform-thickness tube	343.32	159.96	67.99%	10.88
Final designed tube	249.36	190.80	76.52%	10.77

4.2 Straight-line-with-a-slope FD target under oblique impact

For the same thin-walled tube described in the previous example (Sec. 4.1), let us consider the impacting rigid plate positioned at an angle of $15°$ around the z axis, moving at a constant velocity of 5 m/s in the negative y direction (Figure 12). In this example, the progressive collapse is induced using a straight-line-with-a-slope FD target of $f = 160$ kN and $d_t = 0.07$ m. The number of the discrete equidistant points is $m = 700$. Symmetry constraints are included in the x and z directions.
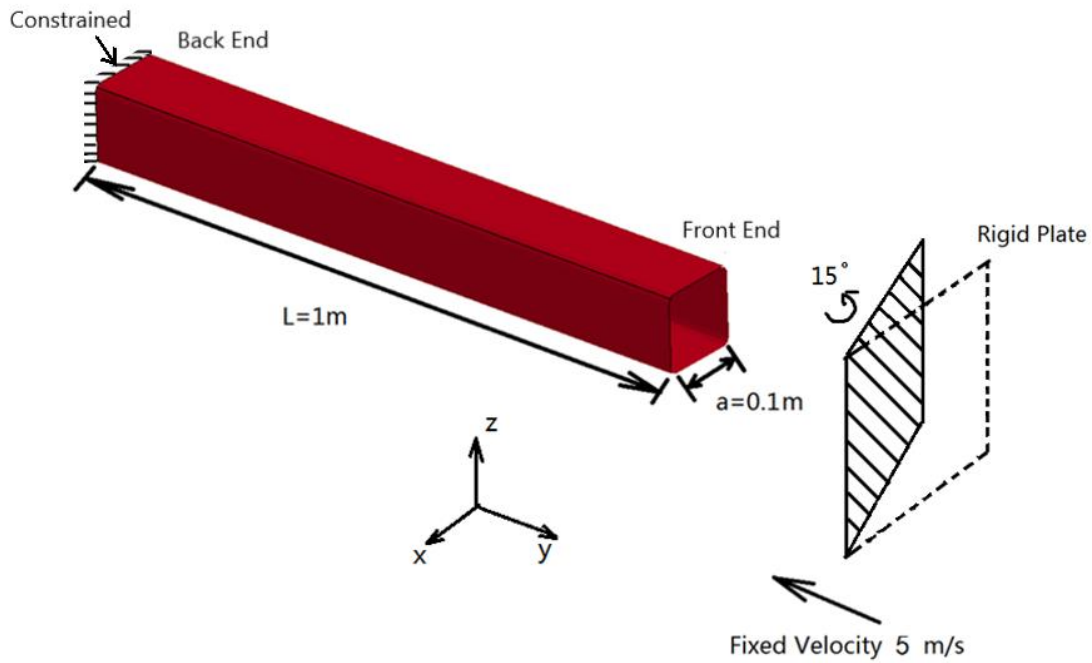
Figure 12: Model setup of the thin-walled square tube under oblique impact.

As before, the initial design is a tube of uniform thickness 3.3 mm. The upper and lower bounds are 6.0 mm and 0.6 mm, respectively. The move limit in the subproblem is $\varepsilon = 0.1$ mm and the convergence number is $N_c = 10$. The evolution of the objective function is shown in Figure 13. Oscillations are observed: the deformation mode in iterations 9,17, and 23 are all global bending. One possible cause is the constant function defining the target FD curve. the optimization is terminated after 25 iterations. The best design is found at iteration 15.
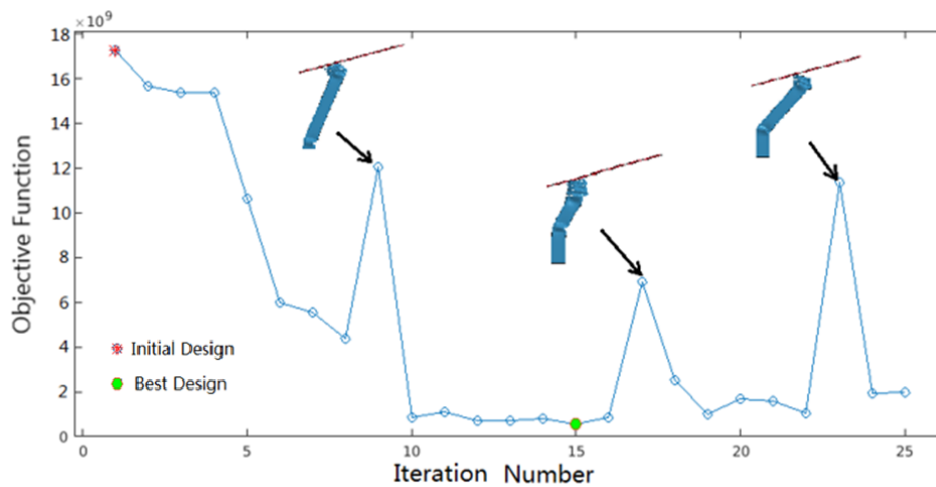
The minimum and maximum thickness values with respect to the number of iterations is shown in Figure 14. The thickness distribution of the final designed tube is shown in Figure 15. In this case, in order to avoid the global bending, the algorithm tries to add material to the tube's back-end thicker; however, this causes a high peak force outside of the target FD curve when the impactor moves to this thicker part. Then the algorithm makes it thinner again, which brings the global bending type deformation back again. The final design has a sufficiently thick back end and progressive collapse is observer.
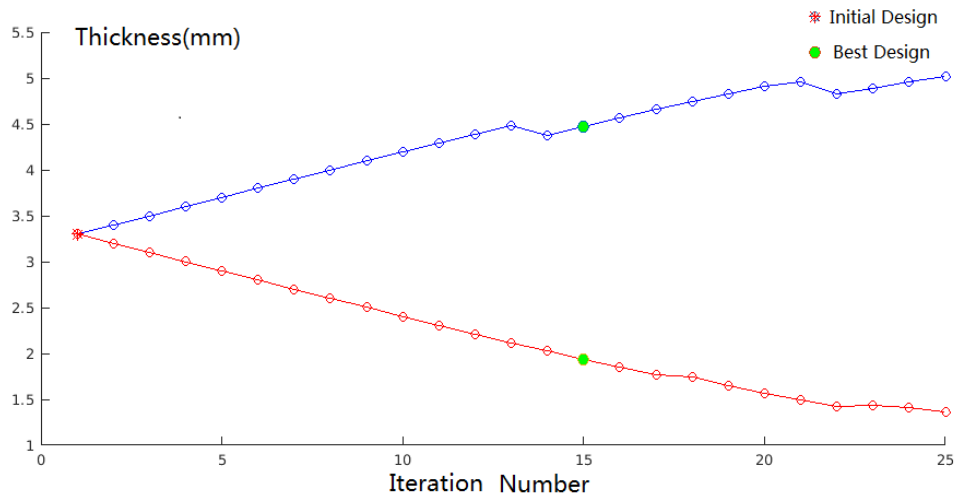

Figure 14: Minimum and maximum thickness values vs. number of iterations for the straight-line-with-a-slope FD target under oblique impact. At convergence, the minimum and maximum thickness values are 1.94 mm and 4.47 mm, respectively.
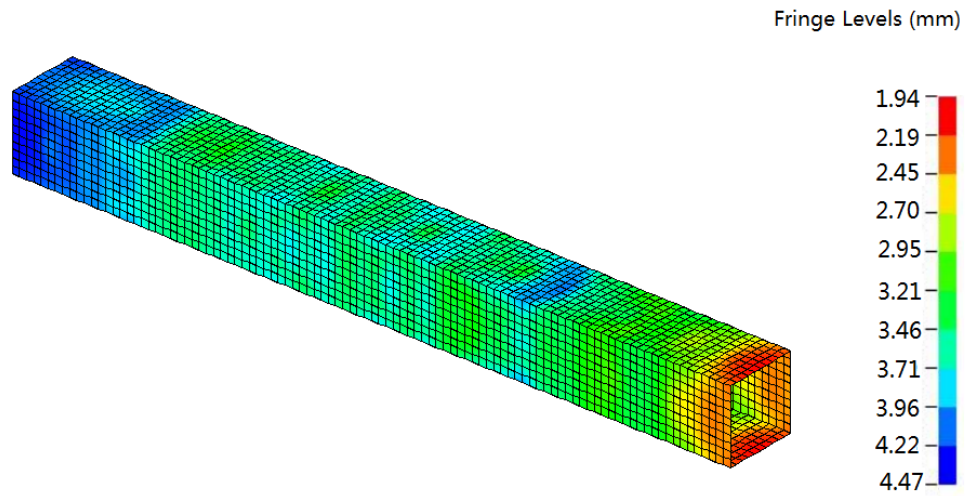
Figure 15: Thickness distribution of the final designed tube for the straight-line-with-a-slope FD target under oblique impact.

Figure 16 shows the global bending of the initial uniform-thickness design and the resulting progressive collapse of the final designed tube. The FD curve of uniform thickness tube and designed tube are shown in Figure 17. For the initial design, a sudden force decrease is observed when global bending occurs, which reduces the energy absorbing capacity of the tube. The final designed tube depicts progressive collapse and maintains higher energy absorbing capacity. The peak force, mean force, CLE, and SEA of the uniform thickness tube and designed tube are listed in Table 3.
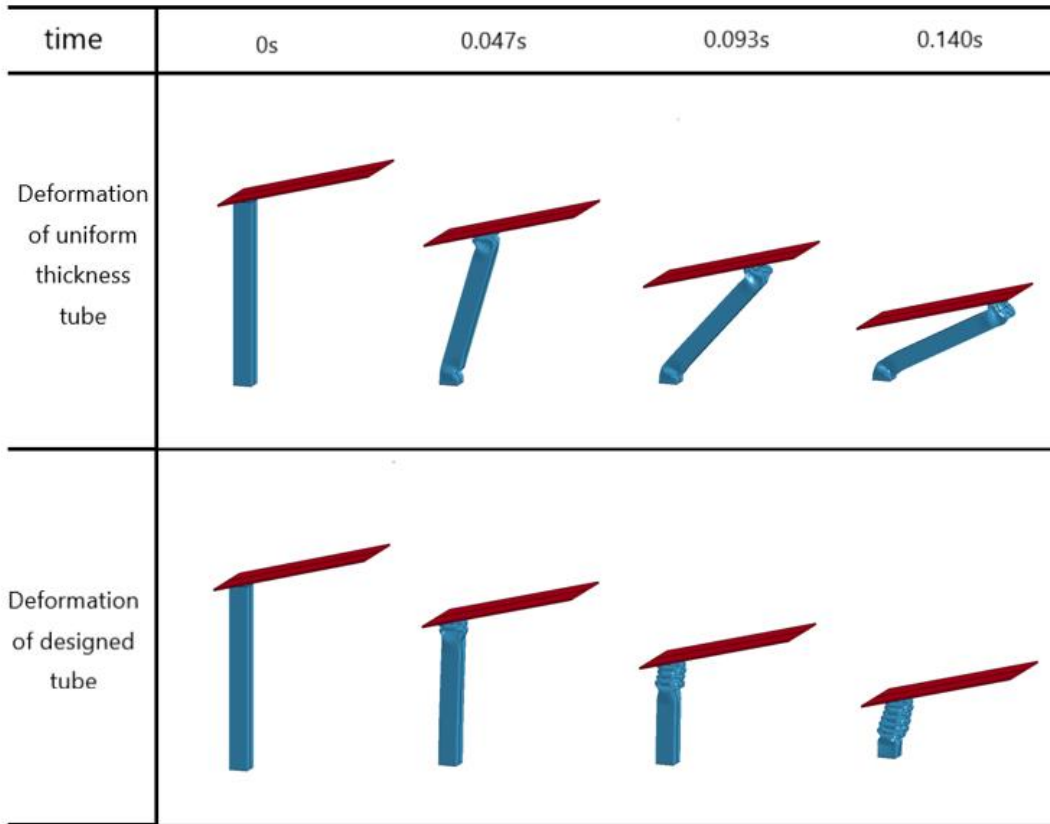
Figure 16: Deformation of the uniform thickness tube vs. the designed tube for the straight-line-with-a-slope FD target under oblique impact.
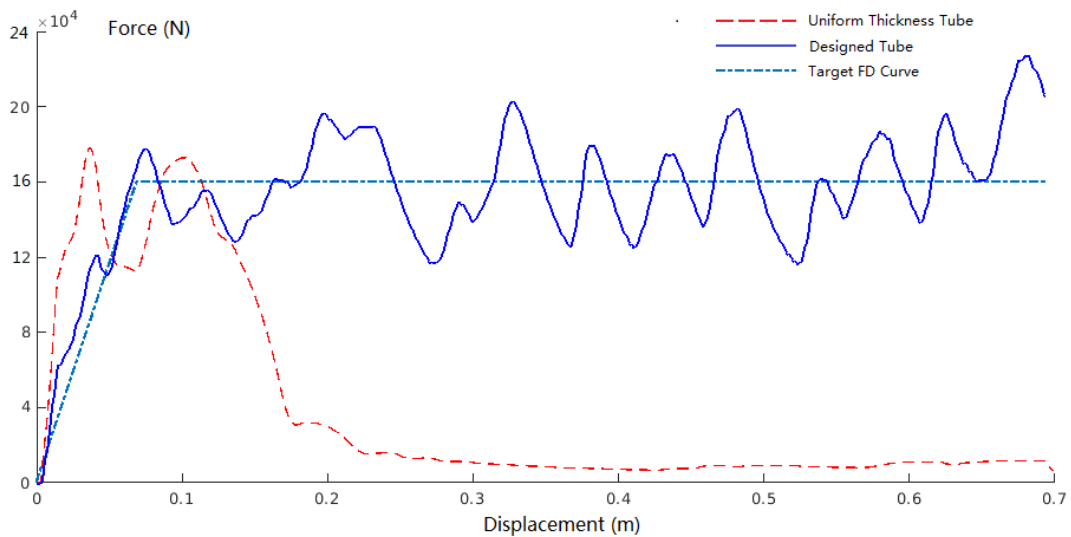

Figure 17: Comparison of the FD response of the initial and final designs for a straight-line-with-a-slope FD target under oblique impact.

Table 3: Performance of the initial uniform-thickness tube and the final designed tube for the straight-line-with-a-slope FD target under oblique impact.

	PCF (kN)	Mean Force (kN)	CLE	SEA (kJ/kg)
Initial uniform-thickness tube	177.92	38.86	21.84%	2.64
Final designed Tube	227.32	154.16	67.82%	9.80

While the numeric result shows a desirable performance, the designed lacks of robustness and a small variation of its thickness, particularly in the back-end, may trigger global bending. In order to avoid this problem, the force of the target curve should be an increasing function of displacement. Therefore, a power-line FD target can be used instead as shown in the next example.

4.3 Power-line FD target under oblique impact

Here, the model and parameters are the same as in the previous examples (Secs. 4.1 and 4.2). The oblique impact is the same described in Sec. 4.2, but a target power-line FD curve is used instead with parameters $f = 200$ kN and $p = 0.4$. The iterative progress of the objective function is shown in Figure 18. Compared with the designed tube in previous example (Sec. 4.2), the convergence is more monotonic and less oscillatory. The algorithm converges after 31 iterations. The collapse observed in the intermediate designs of the previous example did not appear in the deformation progress. The best design is found after 21 iterations. One can find there are no oscillations in the iteration history of the objective function. The minimum and maximum values of thickness variables with respect to the number of iterations are shown in Figure 19 and the thickness distribution of the final designed tube is shown in Figure 20.
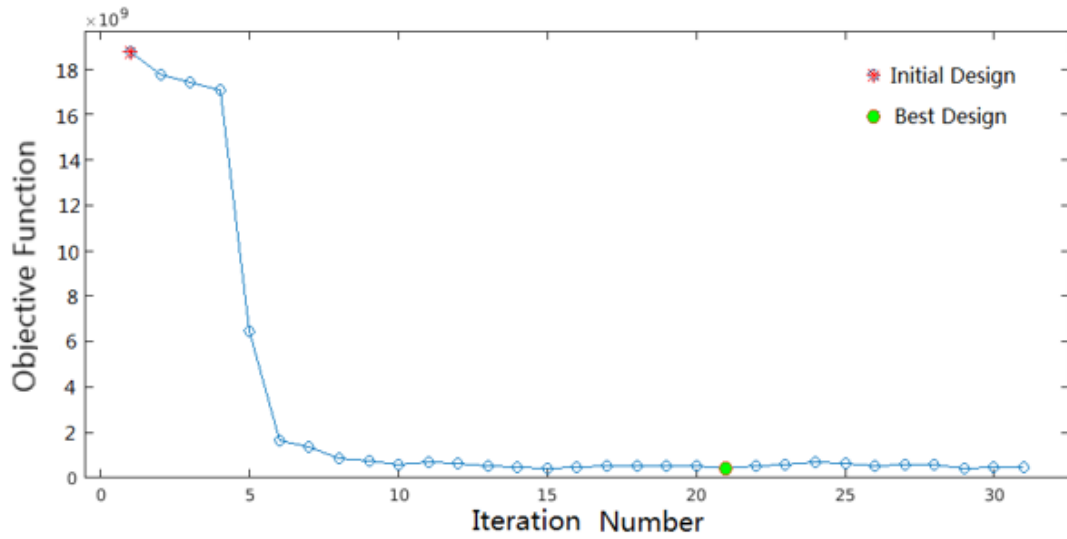
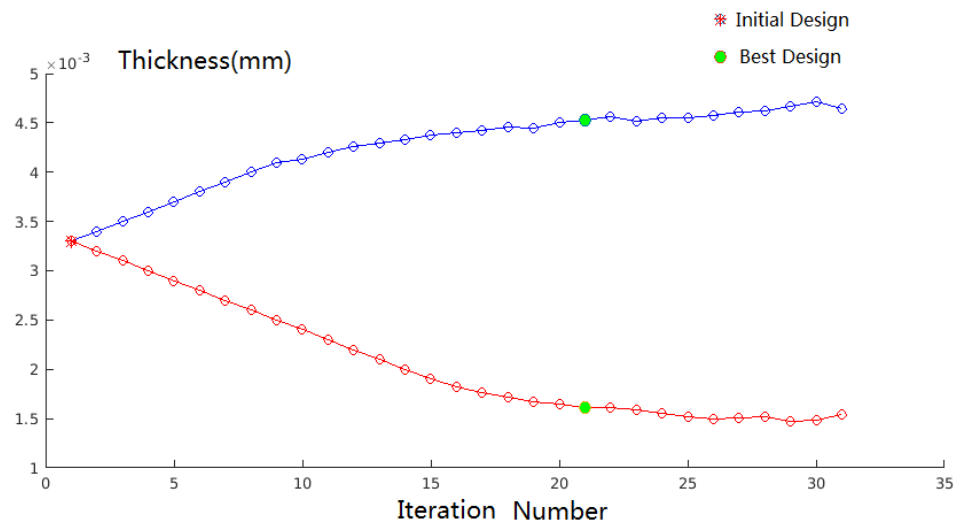Figure 18: Objective function vs. number of iterations for the power-line FD target under oblique impact.

Figure 19: Minimum and maximum thickness values vs. number of iterations for the power-line FD target under oblique impact. At convergence, the minimum and maximum thickness values are 1.61 mm and 4.53 mm, respectively.

Fringe Levels (mm)

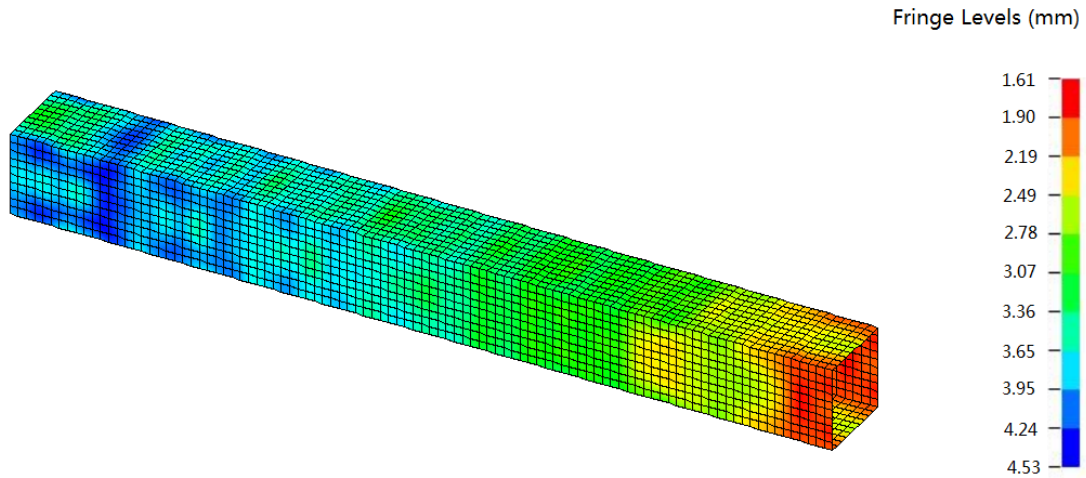1.61
1.90
2.19
2.49
2.78
3.07
3.36
3.65
3.95
4.24
4.53

Figure 20: Thickness distribution of final designed tube for the power-line FD target under oblique impact.

The final designed tube depicts progressive collapse (Figure 21). The FD curves of initial and final designs are shown in Figure 22, showing the response close to the target for the final designed tube. The peak force, mean force, CLE and SEA of the designed tube are listed in Table 4. In comparison to the previous two examples (Tables 2 and 3), the CLE of power-line-target is lower; then, the designed tube using the power line-target FD curve is also lower. According to these examples, the proposed design algorithm is shown to be quite effective.
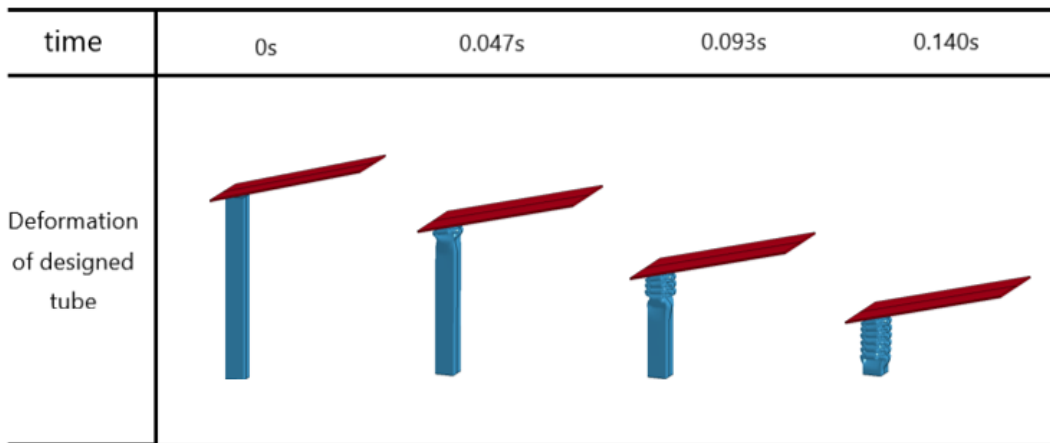

Figure 21: Deformation of the initial uniform-thickness tube vs. the final designed tube for the power-line FD target under oblique impact.
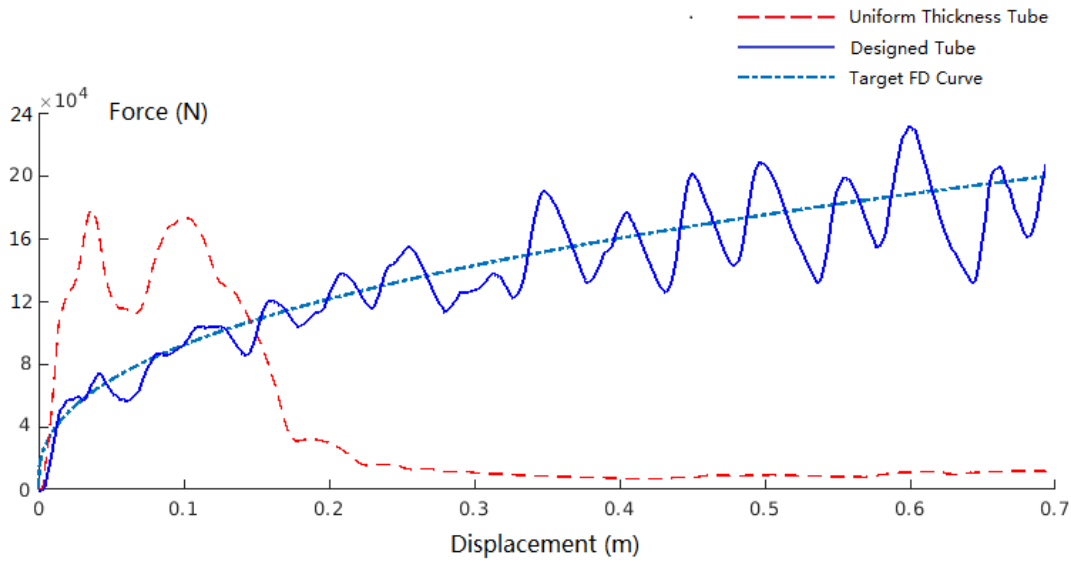
Figure 22: Comparison of the FD curve of the initial and final designs for the power-line FD target under oblique impact.

Table 4: Performance of the initial uniform-thickness tube and the final designed tube for the power-line FD target under oblique impact.

	PCF (kN)	Mean Force (kN)	CLE	SEA (kJ/kg)
Initial uniform-thickness tube	177.92	38.86	21.84%	2.64
Final designed tube	231.52	138.24	59.71%	9.38

5. Conclusion

This work introduces a new heuristic optimization algorithm for the design of thin-walled structures for crashworthiness. The proposed algorithm solves the optimization problem of tracking a target FD curve by dividing such problem into a series of subproblems. At each iteration, an explicit dynamic analysis is performed and a subproblem is solved. By using the relationship between the impact force and structural energy (8), an analytical expression can be derived relating the design variable (thickness) and the derivatives of element energy with respect to the displacement of the impacting body (9 and 13). By solving the subproblem, the algorithm updates thickness distribution

to minimize the error between the structure's FD response and the target FD curve.

Three examples show that the algorithm has the ability to make the FD curve of the optimized structure close to the specified target FD curve on a thin-walled tube with square section. In these examples, the initial design is a thin-walled tube of uniform thickness. In the first example—straight-line FD target under axial impact—the deformation modes of the initial and the final designed tubes are progressive collapse; however, the folds of the designed tube are uniform and the FD curve is closer to the target.

In the remaining two examples, oblique impact is considered with two different targets: straight-line-with-a-slope and power-line FD curves. Under oblique load, the initial tube design with uniform thickness deforms with global bending, losing its energy absorbing capacity; in contrast, the final designed tubes progressive collapse following the target FD curve. In all cases, performance indicators such as PCF, mean force, CLE, and SEA improve according to the FD target. Ongoing applications are carried out with thin-walled tube with different cross-section as well as pillars, rails, and other vehicle components.

A key element of the algorithm is the appropriate way to construct the subproblems, which is solved here by using the structural response information in dynamic analysis. In the subproblem of this research, the energy of each element is only affected by its own thickness changes. This assumption makes the problem simpler and the algorithm computationally efficient. However, the energy of each element has a complex coupling relationship with the thickness of itself and of other elements. This means the structural response information is not fully utilized when constructing subproblems. In this way, the algorithm may lack the ability to explore new deformation modes of complex structures. In further research, how to use this information more sufficiently to build a subproblem will be the essential part of the study. The algorithm can also be extended to other models, such as using different objective functions (maximizing SEA) and different design variables (the shape optimization using the nodes' position as design variables).

6. References

Bandi P., Detwiler D., Schmiedeler J.P., Tovar A. (2015). Design of progressively folding thin-walled tubular components using compliant mechanism synthesis. *Thin-Walled Structures, 95*:208-220.

Baroutaji, A., Sajjia, M., Olabi, A-G (2017). On the crashworthiness performance of thin-walled energy absorbers: Recent advances and future developments. *Thin-Walled Structures*, 118:137-163.

Duddeck, F., S. Hunkeler, P. Lozano, E. Wehrle, D. Zeng (2016) Topology optimization for crashworthiness of thin-walled structures under axial impact using hybrid cellular automata. *Structural and Multidisciplinary Optimization*, 54(3):415-428.

Guler, M.A., Cerit, M.E., Bayram, B., Gerceker, B., Karakaya, E. (2010). The effect of

geometrical parameters on the energy absorption characteristics of thin-walled structures under axial impact loading. *International Journal of Crashworthiness*, 15(4):377-390.

Hallquist J. (2006). LS-DYNA Theoretical Manual, Livermore Software Technology Corporation (LSTC)

Jones N. (1997). Structural Impact, Cambridge University Press, Cambridge, England.

Kim Y.I., Park G.J. (2010). Nonlinear dynamic response structural optimization using equivalent static loads. *Computer Methods in Applied Mechanics & Engineering, 199*(9): 660-676.

Levia J.P. (2004). Topometry Optimization: A New Capability to Perform Element by Element Sizing Optimization of Structures. *AIAA/ISSMO Multidisciplinary Analysis and Optimization Conference*.

Lu, G.X., Yu, T.X. (2003). Energy absorption of structures and materials, M. Woodhead Publishing Limited, Abington Cambridge CB1 6AH, England. pp 26-32.

Mozumder, C., Renaud J.E., Tovar A. (2012). Topometry optimisation for crashworthiness design using hybrid cellular automata. *International Journal of Vehicle Design, 60*(1-2): 100-120.

Mozumder, C, Tovar, A., Renaud, J.E. (2010). Topometry optimization of plastically deformable sheet-metal structure with prescribed force-displacement response for controlled energy absorption. *8th World Congress on Structural and Multidisciplinary Optimization* , Lisbon, Portugal.

Park, G.J. (2011). Technical overview of the equivalent static loads method for non-linear static response structural optimization. *Structural and Multidisciplinary Optimization, 43*(3): 319-337.

Park, G.J., Kang, B.S. (2003). Validation of a structural optimization algorithm transforming dynamic loads into equivalent static loads. *Journal of Optimization Theory & Applications, 118*(1):191-200.

Patel, N.M. (2007). Crashworthiness Design using Topology Optimization. PhD thesis, University of Notre Dame, Indiana.

Patel, N.M., Kang, B.S., Renaud, J.E., Tovar, A. (2009). Crashworthiness design using topology optimization. *Journal of Mechanical Design*, 131(6):061013.

Pedersen, C.B.W. (2003). Topology optimization design of crushed 2d-frames for desired energy absorption history. *Structural and Multidisciplinary Optimization, 25*(5-6), 368-382.

Penninger, C.L., Patel, N.M., Niebur, G.L., Tovar, A., Renaud, J.E. (2013). A fully anisotropic hierarchical hybrid cellular automaton algorithm to simulate bone remodeling. *Mechanics Research Communications, 35*(1):32-42.

Penninger, C.L., Watson, L.T., Tovar, A., Renaud, J.E. (2010). Convergence analysis of hybrid cellular automata for topology optimization. *Structural and*

Multidisciplinary Optimization, 40(1-6): 271-282.

Shin, M.K., Park, K.J., Park, G.J. (2007). Optimization of structures with nonlinear behavior using equivalent loads. *Computer Methods in Applied Mechanics & Engineering, 196*(4):1154-1167.

Tovar, A. (2004). Bone Remodeling as a Hybrid Cellular Automaton Optimization Process. PhD thesis, University of Notre Dame, Indiana.

Tovar, A., Patel, N.M., Niebur, G.L., Sen, M., Renaud, J.E. (2006). Topology optimization using a hybrid cellular automaton method with local control rules. *Journal of Mechanical Design, 128*(6):1205-1216.

Witowski, K., Mullerschon, H., Erhart, A., Schumacher, P., Anakiev, K. (2014) Topology and topometry optimization of crash applications with the equivalent static load method. *13th International LS-DYNA Users Conference*, Dearborn, MI.

Zeng, D., Duddeck, F. (2017) Improved hybrid cellular automata for crashworthiness optimization of thin-walled structures. *Structural and Multidisciplinary Optimization*, 56(1):101-115.